AIMS Materials Science, 4(4): 878-893.
DOI: 10.3934/matersci.2017.4.878
Received: 24 June 2017
Accepted: 08 August 2017
Published: 10 August 2017

http://www.aimspress.com/journal/Materials

Research article

A simple route to linear and hyperbranched polythiophenes containing diketopyrrolopyrrole linking groups with improved conversion efficiency

Chia-Hao Hsieh [1], Wei-Chi Chen [1], Sheng-Hsiung Yang [1,*], Yu-Chiang Chao [2], Hsiao-Chin Lee [2], Chia-Ling Chiang [2], and Ching-Yi Lin [2]

[1] Institute of Lighting and Energy Photonics, National Chiao Tung University, 301 Gaofa 3rd Road, Guiren District, Tainan City 71150, Taiwan R.O.C.
[2] Department of Physics, Chung-Yuan Christian University, No. 200, Chung-Pei Road, Chungli, Taoyuan City 32023, Taiwan R.O.C.

* **Correspondence:** Email: yangsh@mail.nctu.edu.tw; Tel: +886-6-303-2121; Fax: +886-6-303-2535.

Abstract: Two novel polythiophene derivatives with linear or hyperbranched architectures using diketopyrrolopyrrole (DPP) as linking groups as well as normal poly(3-hexylthiophene) (P3HT) were synthesized via the Universal Grignard metathesis polymerization. The molecular weights of the linear polythiophene containing DPP linking moieties are higher than those of P3HT, while molecular weights of the hyperbranched one are smaller. The main decomposition temperatures of polymers were measured at 470 ℃ from TGA experiments. The UV-vis absorption behaviors of the DPP-containing polymers are similar to that of P3HT; moreover, these DPP-containing polythiophenes show distinct PL decay both in solution and thin film states. The electrochemical experiments reveal that the incorporation of DPP groups resulted in lowering HOMO levels of polymers. All polymers were blended with $PC_{61}BM$ and used as active layers for the fabrication of inverted polymer solar cells. The power conversion efficiency of devices based on linear and hyperbranched polythiophenes reached 3.74% and 2.38%, respectively, revealing comparable or even higher efficiency than the one based on normal P3HT.

Keywords: hyperbranched; polythiophene; diketopyrrolopyrrole; inverted polymer solar cells

1. Introduction

Polythiophene (PT) and its derivatives have been extensively utilized for the fabrication of polymer solar cells (PSCs) with moderate power conversion efficiency (*PCE*) in the past decade. The most famous PT derivative, namely poly(3-hexylthiophene-2,5-diyl) (P3HT), was firstly synthesized by McCullough et al. with high regioregularity >95% by metathesis polymerization [1,2]. P3HT has high tendency to form close packing of main chains due to strong π–π interaction, which favors transport and migration of carriers. By applying thermal annealing process, the PSC using the blend of P3HT and [6,6]phenyl-C_{61}-butyric acid methyl ester ($PC_{61}BM$) as the active layer reached a *PCE* value of 4.4% [3]. Apart from P3HT, miscellaneous main-chain and side-chain types of PTs have widely been developed and reported in the literature [4–9]. A novel donor–acceptor PT bearing the C_{60} fullerene pendant has also been synthesized as the photoactive layer [10,11,12]. Most of those PTs belong to alternating copolymers, requiring two monomers tethering with different functional groups to react for copolymerization, such as dibromothiophenes with diboronic esters via the Suzuki-coupling reaction, or dibromo-monomers with bis(trimethyltin)-monomers via the Stille-coupling reaction. These monomers require well-designed transformation of functional groups and careful handling of stoichiometric balance to achieve high molecular weights and good photovoltaic performance of final polymers.

In addition to linear architecture, bridging PTs have also been synthesized by introducing bridging moieties between polymer main chains to study their thermal and optical properties as well as device performance. A terthiophene-bridged P3HT derivative, namely PT-VTThV, was proposed by Li et al. by incorporating divinyl-terthiophene moiety between polymer main chains [13]. The conjugated bridging structure provides an alternative pathway for charge carriers to transport between polymer chains, and the enhancement in hole mobility of the polymer was verified. A *PCE* value of 1.72% for the solar device using PT-VTThV:$PC_{61}BM$ as the active layer was obtained. Another P3HT derivative B-P3HT containing bridging 3,3'-dithiophene moiety was reported by Tu et al. [14]. They found that the hole mobility of B-P3HT was decreased compared with linear P3HT, possibly due to chain distortion brought by the small and rigid 3,3'-dithiophene moiety. The solar devices using B-P3HT:$PC_{61}BM$ blends as the active layer showed *PCE* values of 0.13–2%. Two other hyperbranched conjugated polymers, namely p-3T-TCM and p-4T-TCM, were synthesized by Mangold et al. [15], using 2,3-dithienylthiophene and 2,3,5-trithienylthiophene as bridging cores, respectively. The optimized PSC using p-3T-TCM:$PC_{61}BM$ blend as the active layer revealed an open-circuit voltage (V_{OC}) of 714 mV which was significantly higher than that of P3HT:$PC_{61}BM$ blend. The obtained efficiency of 0.58–0.61% and extra high V_{OC} of hyperbranched polymers show potential application in PSCs. In 2014, our group reported novel hyperbranched PT derivatives containing chlorinated perylene bisimide (PBI) or soft alkyl spacer as bridging moieties [16]. The synthesized polymers showed increased molecular weights and improved thermal stabilities compared with normal P3HT. Photovoltaic devices based on those hyperbranched polymers blended with $PC_{61}BM$ showed *PCE* values of 0.45–0.84% and high V_{OC} values up to 0.70–0.72 V. To be honest, the device performance of those hyperbranched PT derivatives is still low and far beyond practical application, which requires further improvement through chemical modification.

Here we propose new linear and hyperbranched PT derivatives containing diketopyrrolopyrrole (DPP) as linking moieties. DPP possesses highly electron-withdrawing nature and are commonly used for the synthesis of alternating donor–acceptor polymers with low band-gaps [17,18,19]. To

synthesize alternating PTs, dibromo-monomers accompanying with diboronic ester derivatives or bis(trimethyltin)-monomers must be prepared before carrying out the polymerization. In this study, new P3HT derivative were obtained by simply introducing DPP-containing dibromothiophene or two-headed monomers during polymerization of P3HT via the Universal Grignard metathesis polymerization. Normal P3HT was also synthesized according to the same polymerization condition to examine the effect of introducing DPP linking moieties. The thermal, optical, and electrochemical behaviors of the synthesized polymers were investigated via different characterizing techniques. Finally, inverted PSCs based on polymer:$PC_{61}BM$ blends were fabricated and characterized to evaluate the performance of those polymers.

2. Materials and Method

2.1. Characterization Methods

^{1}H- and ^{13}C-NMR spectra were performed on a Bruker Avance 600 MHz NMR spectrometer. Mass spectra were recorded on a Micromass TRIO-2000 GC-MS instrument, using electron impact (EI) or fast atom bombardment (FAB) as ionization source. Gel permeation chromatography (GPC) assembled from a Viscotek VE3850 RI detector and three columns in series were used to measure molecular weights and polydispersity index (PDI) values of polymers relative to polystyrene standards at 32 ℃. Tetrahydrofuran (THF) was used as the eluent to carry out GPC experiments. Fourier-transform infrared (FTIR) spectra were measured on a Nicolet iS-10 spectrometer. Thermogravimetric analysis (TGA) was undertaken on a Seiko TG/DTA 7200 instrument at a heating rate of 20 ℃/min. Differential scanning calorimetry (DSC) was performed on a Seiko DSC 6200 instrument at a heating rate of 10 ℃/min. UV-vis absorption and photoluminescence (PL) spectra were obtained with a Princeton Instruments Acton 2150 spectrophotometer equipped with an 150 W Xenon lamp (USHIO UXL-150S). Cyclic voltammetric measurements of materials were performed on an AUTOLAB PGSTAT30 electrochemical instrument. Indium-tin oxide (ITO) electrodes were used as both the working and counter electrodes, and silver/silver ions (Ag in 0.1 M $AgNO_3$ solution, from Bioanalytical Systems, Inc.) was used as the reference electrode. The polymers were deposited on ITO electrodes and placed in acetonitrile solution containing 0.1 M tetrabutylammonium tetrafluoroborate as the supporting electrolyte with a scan rate of 50 mV/s. Ferrocene was used as an internal standard, and the potential values were obtained and converted to vs Fc/Fc^{+} (ferrocene reference electrode). Atomic force microscopy (AFM) experiments were performed on a Bruker Innova AFM instrument to investigate surface morphologies of polymer:$PC_{61}BM$ blend films. The current density-voltage (J-V) characteristics of photovoltaic devices were taken using a Keithley 2400 source measurement unit under an AM 1.5G exposure from a Yamashito Denso YSS-150AA solar simulator in ambient environment. The external quantum efficiency (EQE) measurements were performed on an assembled apparatus in the laboratory, comprising a solar simulator (Oriel 9600, 150W), the monochromator (Cornerstone^{TM} 130) and the optical power meter (818-UV/DB).

2.2. Synthesis of Monomers

The synthetic routes to monomers **M1** and **M2** are shown in Scheme 1. The preparation of intermediates **(1)** and **(2)** as well as monomers **M1** and 2,5-dibromo-3-hexylthiophene (**M3**) was

referred to the previous literature [20,21]. The detailed synthetic procedure of **M2** is described as follows.

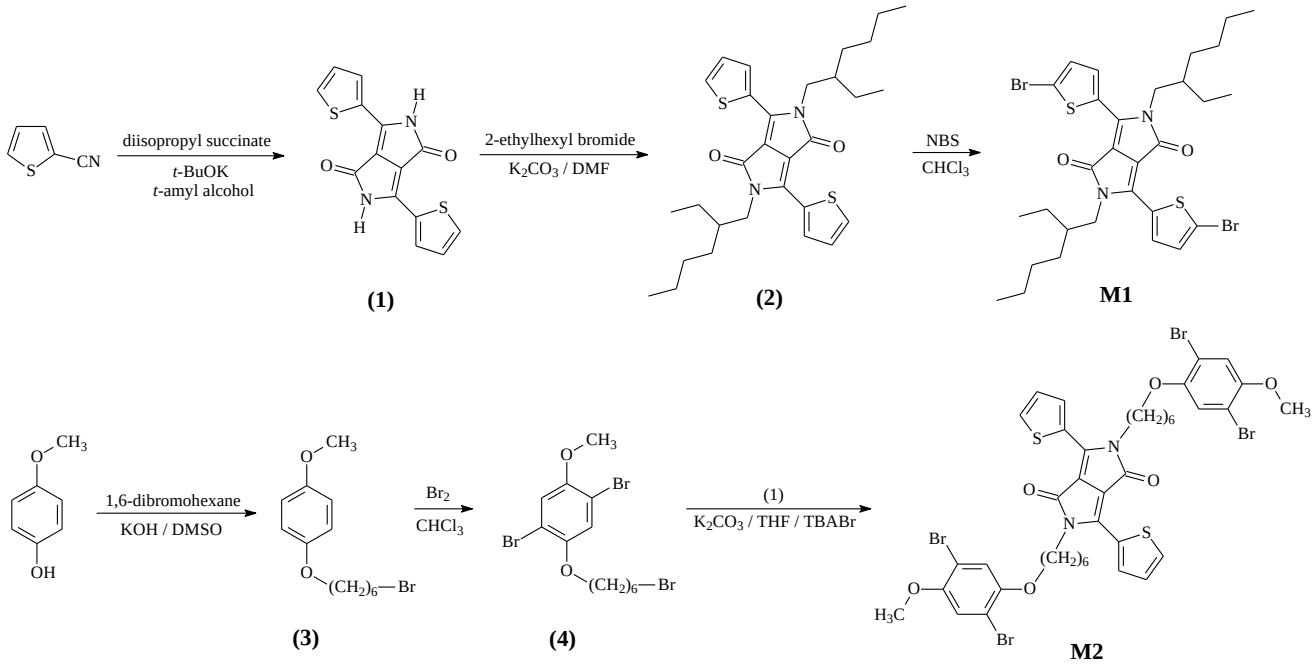

Scheme 1. Synthesis of the monomers **M1** and **M2**.

1-(6'-Bromohexyloxy)-4-methoxybenzene (3). A mixture of 4-methoxyphenol (10.0 g, 85.58 mmol), 1,6-dibromohexane (60.0 g, 245.9 mmol), potassium hydroxide (6.0 g, 106.95 mmol) and dimethyl sulfoxide (DMSO) (100 mL) was stirred at room temperature for 6 hr. The mixture was then extracted with dichloromethane (DCM) and water, and the organic phase was dried with anhydrous magnesium sulfate ($MgSO_4$). The crude product was concentrated in vacuo and purified by column chromatography (silica gel, using DCM:hexane = 2/1 in volume ratio as the eluent) to give a white solid (15.0 g, 65%). ^{1}H-NMR ($CDCl_3$, ppm): 1.46–1.51 (m, 4H, $-OCH_2CH_2(C\underline{H}_2)_2-CH_2CH_2Br$), 1.76–1.81 (m, 2H, $-C\underline{H}_2CH_2Br$), 1.87–1.91 (m, 2H, $-OCH_2C\underline{H}_2-$), 3.40–3.44 (t, J = 6.9 Hz, 2H, $-C\underline{H}_2Br$), 3.77 (s, 3H, $-OC\underline{H}_3$), 3.90–3.93 (t, J = 6.3 Hz, 2H, $-OC\underline{H}_2-$), 6.83 (s, 4H, aromatic protons). ^{13}C-NMR ($CDCl_3$, ppm): 25.32, 27.94, 29.21, 32.70, 33.78, 55.75, 68.41, 114.65, 115.46, 153.22, 153.75. MASS (EI): m/z 287.

1-(6'-Bromohexyloxy)-2,5-dibromo-4-methoxybenzene (4). A mixture of compound **(3)** (5.0 g, 17.41 mmol), a small amount of iron powder and chloroform (100 mL) was stirred at 0 ℃ in an ice-water bath. Bromine (8.0 g, 50.0 mmol) was then slowly added to the mixture and stirred at room temperature for 12 hr. The reaction mixture was then extracted with ethyl acetate (EA) and sodium thiosulfate aqueous solution for three times, and the organic phase was dried with anhydrous $MgSO_4$. The crude product was concentrated in vacuo and purified by column chromatography (silica gel, using EA/hexane = 1/14 in volume ratio as the eluent) to yield a white solid (5.0 g, 65%). ^{1}H-NMR ($CDCl_3$, ppm): 1.52–1.54 (m, 4H, $-OCH_2-CH_2(C\underline{H}_2)_2CH_2CH_2Br$), 1.81–1.83 (m, 2H, $-C\underline{H}_2CH_2Br$), 1.88–1.91 (m, 2H, $-OCH_2C\underline{H}_2-$), 3.41–3.44 (t, J = 6.9 Hz, 2H, $-C\underline{H}_2Br$), 3.84 (s, 3H, $-OC\underline{H}_3$), 3.95–3.97 (t, J = 6.3 Hz, 2H, $-OC\underline{H}_2-$), 7.09 (s, 2H, aromatic protons). ^{13}C-NMR

($CDCl_3$, ppm): 25.19, 27.81, 28.92, 32.64, 33.74, 56.99, 70.06, 110.41, 111.27, 117.01, 118.65, 150.04, 150.55. MASS (EI): m/z 445.

2,5-Bis[6-(2,5-dibromo-4-methoxyphenyl)hexyloxy]-3,6-dithiophen-2-yl-pyrrolo[*3,4-c*]pyrrole-1,4-dione (M2). A mixture of compounds **(1)** (1.0 g, 3.33 mmol), **(4)** (3.3 g, 7.47 mmol), K_2CO_3 (3.83 g, 27.71 mmol), tetrabutylammonium bromide (TBABr) (0.13 g, 0.4 mmol), 18-crown-6 (0.1 g, 0.38 mmol) and *N*,*N*-dimethylformamide (50 mL) was refluxed at 145 ℃ for 24 hr under nitrogen atmosphere. After cooling to room temperature, the mixture was poured into 400 mL of water and filtered. The filter solid was washed with water for several times and then purified by column chromatography (silica gel, using DCM as the eluent) to give a dark red solid (1.0 g, 29%). ^{1}H-NMR ($CDCl_3$, ppm): 1.5 (m, 4H, –$NCH_2CH_2CH_2C\underline{H}_2CH_2CH_2O$–), 1.56 (m, 4H, –$NCH_2CH_2C\underline{H}_2CH_2$–$CH_2CH_2O$–), 1.7–1.9 (m, 8H, –$NCH_2C\underline{H}_2CH_2CH_2C\underline{H}_2CH_2O$–), 3.83 (s, 6H, –$OC\underline{H}_3$), 3.94 (m, 4H, –$NCH_2CH_2CH_2CH_2CH_2C\underline{H}_2O$–), 4.09 (m, 4H, –$NC\underline{H}_2CH_2CH_2CH_2$–$CH_2CH_2O$–), 7.07 (s, 4H, aromatic protons), 7.28 (s, 2H, aromatic protons), 7.63 (s, 2H, aromatic protons), 8.91 (s, 2H, aromatic protons). ^{13}C-NMR ($CDCl_3$, ppm): 25.63, 26.52, 28.96, 29.85, 42.04, 56.98, 70.11, 107.68, 110.37, 111.28, 116.99, 118.65, 128.64, 129.68, 130.72, 135.30, 139.99, 150.06, 150.51, 161.35. MASS (FAB): m/z 1029.

2.3. Synthesis of Polymers

The syntheses of linear polymer **P1** and hyperbranched polymer **P2** are depicted in Scheme 2, which were polymerized via the Universal Grignard metathesis polymerization [22]. The molar ratio of isopropylmagnesium chloride–lithium chloride (i-PrMgCl·LiCl) complex to monomer was controlled to 1.3:1. The molar ratio of the catalyst 1,2-bis(diphenyl-phosphinoethane)nickel(II) chloride ($Ni(dppp)Cl_2$) to monomer was controlled to 0.005:1. The feed ratio of monomers **M1** (or **M2**) to **M3** was selected to 0.05:1. The detailed synthetic procedures of the polymer **P1** were given as an example.

P1: to a mixture of **M1** (0.104 g, 0.15 mmol) and **M3** (1.0 g, 3.07 mmol) in anhydrous THF (40 mL) was added 1 M i-PrMgCl·LiCl (4 mL, 4.0 mmol) using syringe under nitrogen atmosphere. The reaction mixture was heated to 80 ℃ and stirred for 2 hr. A dispersion of $Ni(dppp)Cl_2$ (9.0 mg, 1.66×10^{-2} mmol) in anhydrous THF (20 mL) was injected into the reaction mixture and stirred at 80 ℃ for 3 hr. The resulting solution was then poured into methanol (250 mL) and stirred for 1 hr. The crude product was collected by filtration and re-precipitated in hexane for several times to give a purple-black solid (0.33 g, 63%). ^{1}H-NMR ($CDCl_3$, ppm): 0.9–2.0 (m, alkyl–H), 2.56–2.8 (t, thiophene–$C\underline{H}_2$–), 4.16 (t, imide–$C\underline{H}_2$–), 6.9–7.1 (br, thiophene–H). FTIR (cm^{-1}): 3055, 2955, 2922, 2853, 1635, 1509, 1455, 819.

P2: by following the synthetic procedure of **P1** and using **M2** (0.158 g, 0.152 mmol), **M3** (1.0 g, 3.07 mmol), i-PrMgCl·LiCl (4 mL, 4.0 mmol) and $Ni(dppp)Cl_2$ (9.0 mg, 1.66×10^{-2} mmol) as starting materials, **P2** was obtained as a purple-black solid (0.16 g, 31%). ^{1}H-NMR ($CDCl_3$, ppm): 0.9–2.0 (m, alkyl–H), 2.58–2.8 (t, thiophene–$C\underline{H}_2$–), 3.78 (s, –O–$C\underline{H}_3$), 3.82–3.84 (m, –O–$C\underline{H}_2$– and imide–$C\underline{H}_2$–), 6.9–7.1 (br, aromatic–H). FTIR (cm^{-1}): 3053, 2954, 2922, 2851, 1638, 1508, 1451, 820.

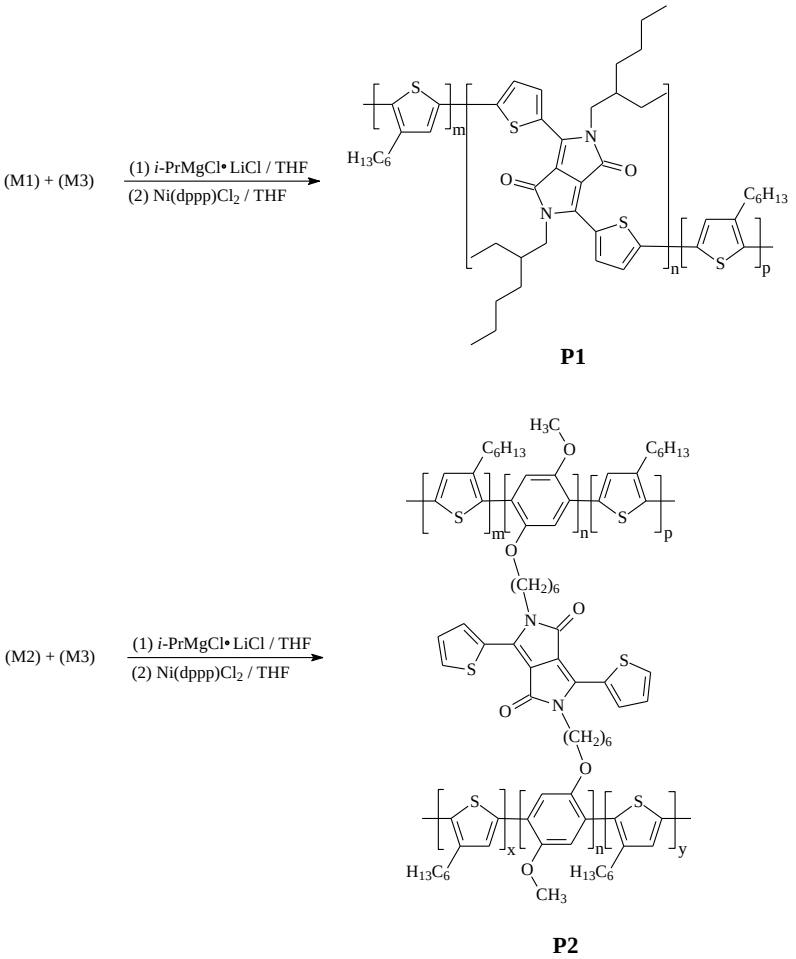

Scheme 2. Synthesis of the polymers **P1**and **P2**.

2.4. Device Fabrication

P3HT, **P1**, and **P2** were blended with $PC_{61}BM$ (1:1 in weight ratio) individually in *o*-dichlorobenzene (*o*-DCB) at a total concentration of 40 mg/mL. 30 μL of 1,8-diiodooctane (DIO) was added in the above solutions to improve morphology of resulting blend films. The solutions were treated with ultrasonication at 70 ℃ for 30 min for better dissolution. The solutions were then filtered with 0.22 μm PTFE filters before use. Inverted photovoltaic devices with the configuration of ITO/ZnO nanorod arrays/ionic PF/polymer:$PC_{61}BM$/PEDOT:PSS/WO_3/Au were fabricated. The ZnO nanorod arrays were prepared according to the previous report and used as the electron transporting layer (ETL) [23]. An ultra-thin ionic PF layer was deposited on top of ZnO nanorod arrays from its dilute solution (0.1 wt% in acetonitrile) before depositing active layers. The ionic PF was prepared according to the previous report [24]. The active layers of polymer:$PC_{61}BM$ (120 nm) were prepared by spin-coating from their solutions at 1000 rpm for 30 sec, followed by solvent annealing in a covered glass petri dish at 60 ℃ for 5 min and dried in a vacuum oven at 90 ℃ for 30 min. Poly(3,4-ethylenedioxythiophene):poly(styrene sulfonate) (PEDOT:PSS) (CleviosTM P VP AI 4083) and tungsten trioxide (WO_3) layers were sequentially deposited on top of active layers. The WO_3 layer was obtained from spin-coating tungsten(V) ethoxide solution (0.1 wt% in anhydrous

ethanol) into thin film, followed by hydrolysis in air for 15 min. Finally, 100 nm of gold electrodes were deposited as the anode by thermal evaporation at a pressure of 8×10^{-6} torr. The area of active layers is 4 mm^2.

3. Results and Discussion

3.1. Synthesis and Characterization of Polymers

In this research, linear PT derivative **P1** and hyperbranched **P2** by were synthesized by incorporating DPP-containing monomers **M1** and **M2**, respectively, during polymerization of P3HT via the Universal Grignard metathesis. Normal P3HT was also synthesized from its monomer **M3** under the same reaction condition for comparison. For polymer **P1**, DPP moieties are randomly incorporated into P3HT main chains to improve electron transport and dissociation of carriers. For polymer **P2**, both heads in **M2** serve as polymerizable monomers to extend polymer chains, forming hyperbranched architectures of final polymers. The feed ratio of monomers **M1** (or **M2**) to **M3** is controlled to be 0.05:1 to ensure successful incorporation of DPP moieties and sufficient solubility of final polymers in common organic solvents, such as THF, chlorobenzene, and *o*-DCB. The number-average molecular weight (M_n), weight-average molecular weight (M_w), and PDI values of all synthesized polymers were determined by GPC. The M_n and M_w values of **P1** are 2.54×10^4 and 6.23×10^4 g/mol, respectively, with a PDI value of 2.45. Moreover, the M_n and M_w values of **P2** are 2.14×10^4 and 3.92×10^4 g/mol, respectively, with a smaller PDI value of 1.83. Meanwhile, the M_n, M_w and PDI values of synthesized P3HT were also measured to be 2.68×10^4, 4.87×10^4 g/mol and 1.81, respectively. It is seen that the molecular weight and PDI value of **P1** are somewhat larger than those of P3HT and **P2**. Due to the fact that linear polystyrenes are used as the standards to construct the calibration curve, we consider that the measured molecular weight of branched **P2** could be overestimated. Besides, it is reported that hyperbranched polymers have more densely packed structures, resulting in smaller hydrodynamic volume compared to those linear ones [25]. Hence, we speculate that the difference in molecular weights of polymers is affected by the polymer architecture and experimental method that we have for GPC measurements. The spectroscopic characterizations including NMR and FT-IR techniques were carefully carried out for all synthesized polymers. Besides, these polymers possess sufficient solubility in *o*-ODCB and can be cast into free-standing thin films for further investigations.

3.2. Thermal Properties

The TGA thermograms of the synthesized polymers **P1**, **P2** and P3HT are depicted in Figure 1(a). The main decomposition temperatures (T_d) due to thermal degradation of polymer main chains are found around 470 ℃, which is consistent with the previous literature [16,26]. A slight first-stage weight loss around 350 ℃, possibly due to the break of alkyl side chains or spacers, is also observed and in good accordance with our previous work [16]. Besides, we notice that this first-stage weight loss can be suppressed by introducing DPP moiety on P3HT, indicating that the incorporation of rigid DPP moieties helps to improve thermal stability of the synthesized PT derivatives.

The glass transition temperature (T_g) and melting temperature (T_m) of the synthesized polymers were determined by DSC. Several research groups have studied the thermal transition behaviors of

P3HT; different T_g values of P3HT ranging from −14 to 110 ℃ [27–30], and T_m values in the range of 200–230 ℃ were reported in the literature [31,32]. This is understandable since the measurement of T_g and T_m is strongly dependent on the qualities and sources of polymers as well as experimental parameters. In this research, polymerization conditions for all polymers were carefully controlled to examine the effect of DPP linking moieties on thermal transition behaviors of final polymers. The DSC thermograms of the polymers **P1**, **P2**, and P3HT are shown in Figure 1(b). The T_g of the synthesized **P1**, **P2**, and P3HT in this study are observed at 72, 67, and 55 ℃, respectively. It is seen that DPP-containing derivatives show lower T_g values compared with P3HT. This can be attributed to less close packing of PT main chains by inserting rigid and bulky DPP moieties. **P2** possesses the lowest T_g value due to its smallest molecular weights among three polymers. Furthermore, the T_m of the synthesized **P1**, **P2**, and P3HT are found at 231, 230, and 215 ℃, respectively. Here again, **P2** shows the lowest T_m value because of its less packed polymer chains and smaller molecular weights. As for the polymer **P1**, although its T_m value is close to that of P3HT, the broader melting peak indicates more disordered main chains of **P1** by introducing DPP moieties compared with the regular homopolymer P3HT.

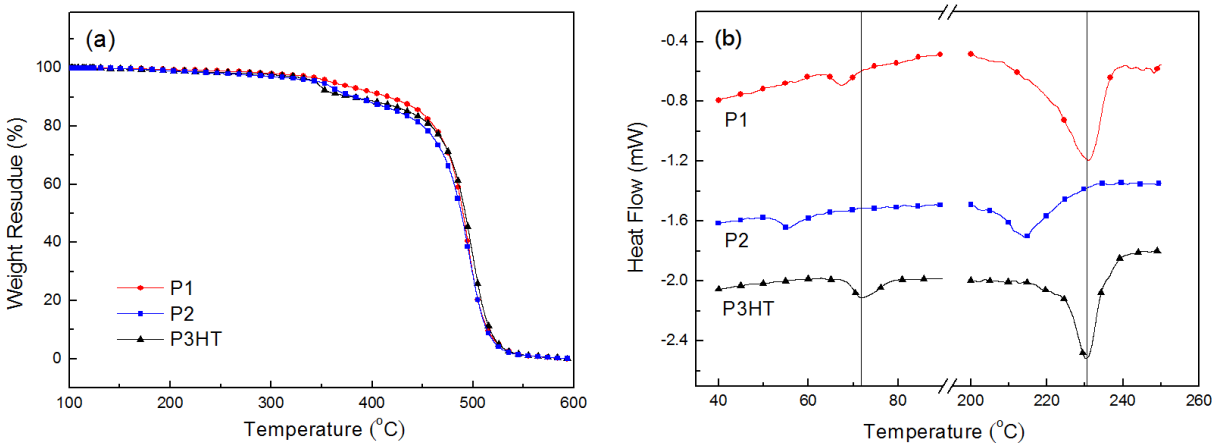

Figure 1. (a) TGA and (b) DSC thermograms of **P1**, **P2** and P3HT.

3.3. Optical Properties

The UV-vis absorption spectra of all polymers in solution or thin film state are shown in Figure 2. *o*-DCB is selected as solvent for optical measurement since it is also used for the preparation of blend solutions to fabricate photovoltaic devices in this study. In Figure 2(a), the absorption band centered at 460 nm are observed for **P1** and P3HT in *o*-DCB, corresponding to π–π* transition along conjugated main chains. Besides, **P2** reveals a slightly blue-shifted absorption maximum at 454 nm. This can be explained by the bridging architecture of **P2** that forms twisted polymer chains to reduce the effective conjugation length. Figure 2(b) shows the absorption bands of all three polymers ranging from 400 to 650 nm in thin film state, revealing three vibronic absorption bands located at 527, 552 and 602 nm. The wavelengths at 527 and 552 nm come from π–π* transition along shorter and longer conjugated polymer chains, respectively [32]. The shoulder band at 602 nm is related to aggregates of polymer chains in thin film state [33]. It is seen that the absorption behaviors of the synthesized polymers in this study are similar to the regioregular P3HT reported in the

literatures [21,27,33]. Moreover, we notice some differences in absorption between hyperbranched **P2** and linear polymers P3HT and **P1**. For P3HT and **P1**, both spectral shapes are quite similar and the intensity of longer conjugation at 552 nm is stronger than the shorter one at 527 nm, as shown in Figure 2(b). Apparently, the two polymers P3HT and **P1** own close conjugation length in thin film state. On the contrary, **P2** shows stronger absorption at shorter wavelength of 527 nm, and its absorption shoulder at 602 nm is weaker than other two polymers. This could be due to the insertion of bridging DPP moieties that twist polymer chains and reduce effective conjugation length. The weaker absorption shoulder band implies hindered interaction and less packing between polymer chains, which may affect the charge transport and conversion efficiency of solar devices. The optical bandgaps (E_g) of polymers are estimated to be 1.89–1.91 eV from the absorption edge of their UV-vis absorption spectra, as shown in Figure 2(b).

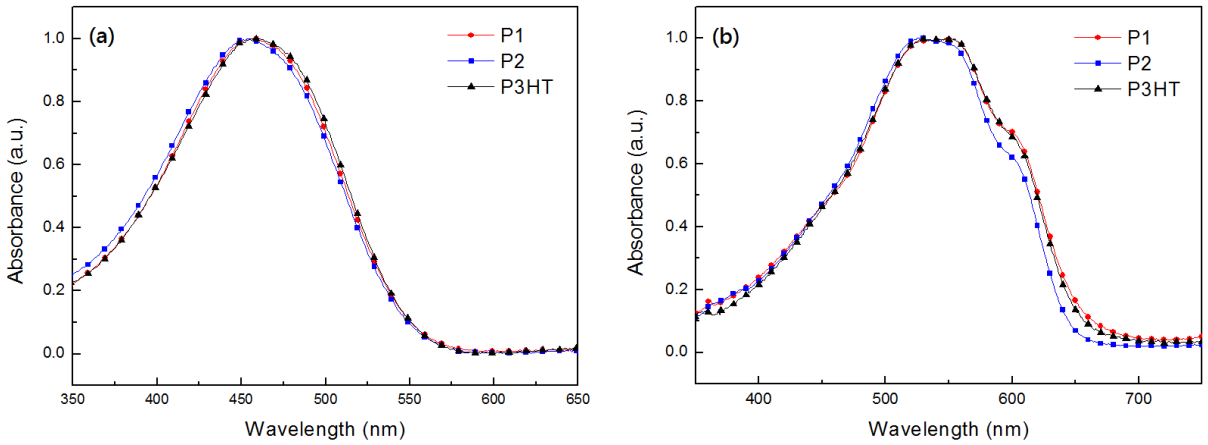

Figure 2. UV-vis absorption spectra of **P1**, **P2** and P3HT in (a) *o*-DCB and (b) thin film state.

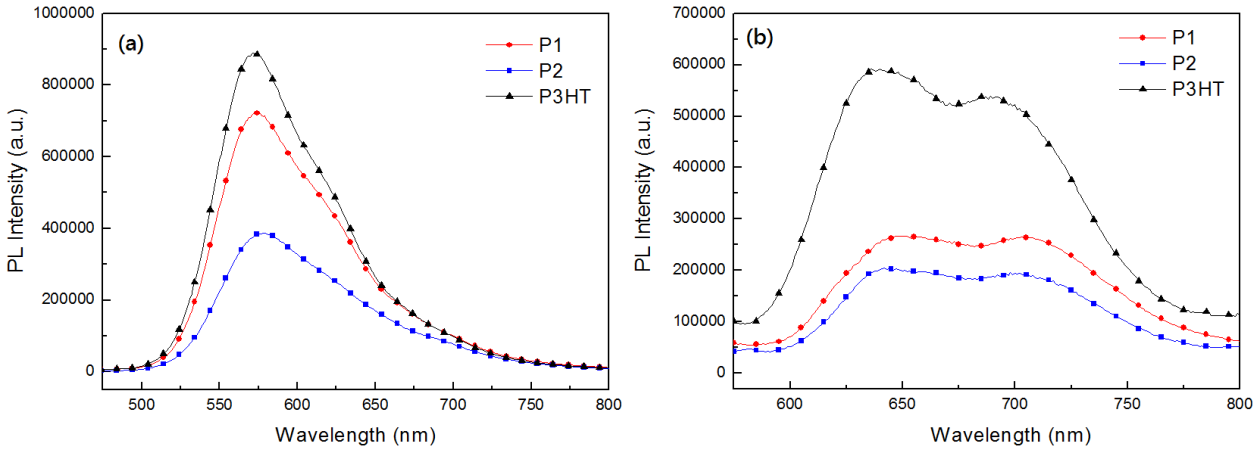

Figure 3. PL spectra of **P1**, **P2** and P3HT in (a) *o*-DCB and (b) thin film state.

The original PL emission spectra of polymers were depicted in Figure 3, which were obtained by excitation of samples at 460 nm in solution and 552 nm in solid state. The main emission band of all polymers is observed at 588 nm in *o*-DCB that is not affected by introducing DPP moieties. The vibronic shoulder band arised from interchain interaction can also be found around 635 nm for all

polymers in Figure 3(a). Turning to PL emission spectra in Figure 3(b), two clear emission maxima around 650 and 700 nm are observed for all polymers in thin film state, which are attributed to intra- and inter-chain emissive behaviors, respectively [33,34]. Besides, two DPP-containing polymers **P1** and **P2** show distinct PL decay both in solution and thin film states compared to normal P3HT. This phenomenon implies a more effective transport process for carriers instead of recombination process to emit light, which has been reported in the previous reports [9,16,35]. It is noted that all samples were prepared according to the same standard, i.e., the same concentration in *o*-DCB and thickness in film.

3.4. Electrochemical Properties

Figure 4 shows the cyclic voltammograms of the synthesized polymers in the oxidation process. The oxidation onset (E_{OX}) of P3HT is found at 0.81 V, corresponding to its highest-occupied molecular orbital (HOMO) of −5.21 eV calculated from the semi-empirical equations [16]. The HOMO of our synthesized P3HT is close to several previous reports, including values of −5.2 [4], −5.1 [16,36,37,38], and −4.9 eV [39]. Here again, the determination of the HOMO of a certain P3HT can be varied with different material sources and experimental parameters. In our CV experiments, we carefully controlled all parameters in the same condition, such as the supporting electrolyte, scan rate and working/counter electrodes, to verify the influence of DPP moieties on polymers. The DPP-containing polymers **P1** and **P2** show higher E_{OX} at 0.89 and 0.84 V, indicating their HOMO levels of −5.29 and −5.24 eV, respectively. The lower HOMO levels of DPP-containing polymers compared with P3HT is resulted from the incorporation of electron-withdrawing DPP groups. The electrochemical properties of **P1**, **P2** and P3HT are summarized in Table 1. It is known that lower HOMO levels of polymers bring benefits of increasing V_{OC} values for solar devices, since V_{OC} can be determined from the energy difference between LUMO of electron acceptor $PC_{61}BM$ (LUMO = −4.3 eV) and HOMO of electron-donor polymers [35,40,41]. Combining the results of PL decay and lower HOMO levels, the synthesized DPP-containing **P1** and **P2** in this study may show comparable or even higher photovoltaic performance compared with normal P3HT.

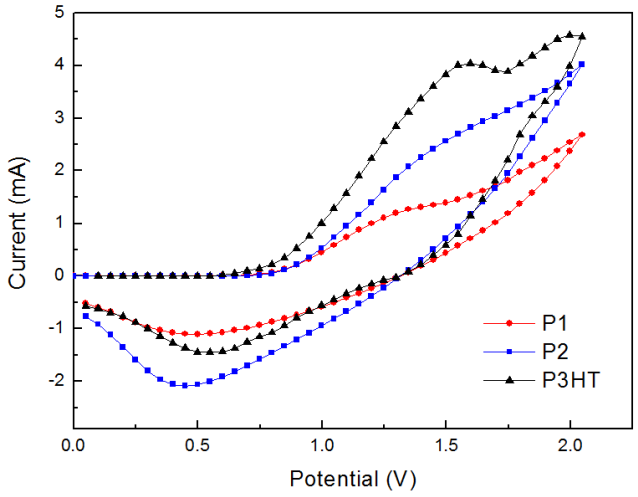

Figure 4. Cyclic voltammograms of **P1**, **P2** and P3HT in the oxidation scan.

Table 1. Electrochemical properties of **P1**, **P2** and P3HT.

Polymer	E_{OX} (V) [a]	HOMO (eV) [b]	LUMO (eV) [c]	Eg (eV) [d]
P1	0.89	−5.29	−3.4	1.89
P2	0.84	−5.24	−3.34	1.9
P3HT	0.81	−5.21	−3.31	1.89

[a] data from CV experiments in the oxidation scan;
[b] HOMO = $-|E_{OX} + 4.4|$;
[c] LUMO = $-|\text{HOMO} + E_g|$;
[d] data from the edge of the absorption spectra in film state.

3.5. Photovoltaic Properties

Inverted solar cells with the configuration of ITO/ZnO nanorod arrays/ionic PF/polymer:$PC_{61}BM$/PEDOT:PSS/WO_3/Au were fabricated and evaluated. The synthesized polymers **P1**, **P2** and P3HT were used as the electron donor, while commercial $PC_{61}BM$ was used as the electron acceptor to form the active layer. ZnO nanorod arrays were adopted as the ETL for the fabrication of inverted solar cells [42]. To improve contact between inorganic ZnO nanorods and organic polymer:$PC_{61}BM$ blend layer, a thin layer of ionic PF containing trimethylammonium hexafluorophosphate ($–N^+(CH_3)_3PF_6^-$) groups were deposited on top of ZnO nanorods, which was also used in our previous study [23]. Moreover, a thin layer of WO_3 was inserted between PEDOT:PSS and Au electrode to act as hole extraction layer to achieve higher conversion efficiency [43,44]. Apart from WO_3, one may choose other metal oxide buffer layers for efficient and stable polymer solar cells, such as nickel oxide, molybdenum trioxide, vanadium oxide and rhenium oxide [45]. The device parameters, including V_{OC}, short-circuit current density (J_{SC}), fill factor (*FF*) and *PCE* of PSCs based on **P1**, **P2** and P3HT are summarized in Table 2, and corresponding current density-voltage characteristics as well as EQE spectra versus wavelength are shown in Figure 5. The optimized inverted solar device based on **P1**:$PC_{61}BM$ blend showed V_{OC}, J_{SC}, *FF*, and *PCE* values of 0.57 V, 16.21 mA/cm^2, 40%, and 3.74%, respectively, which were significantly higher than those of the reference device using P3HT:$PC_{61}BM$ in this study. In other words, the introduction of DPP moieties enhances the photovoltaic properties of P3HT. Besides, the device using hyperbranched **P2**:$PC_{61}BM$ as the active layer showed V_{OC}, J_{SC}, *FF*, and *PCE* values of 0.58 V, 11.29 mA/cm^2, 37%, and 2.38%, respectively. It can be seen that the devices using **P1** and **P2** as the electron donor showed larger V_{OC} than the one of normal P3HT. This is reasonable since the deeper HOMO levels are found for polymers **P1** and **P2**, as discussed in the previous part. The device results also show an increase in V_{OC} for hyperbranched PTs that is in accordance with previous literatures [15,16], although the increment is less significant. From EQE spectra of three solar devices in Figure 5(b), it is also seen that **P1** possesses the highest EQE from 300 to 650 nm, indicating the best J_{SC} value among three polymers. Comparing the EQE spectra of **P2** and P3HT, the intensity of **P2** around 600 nm is lower and the curve drops sharply, making its final J_{SC} and *PCE* value smaller than normal P3HT. The comparison of photovoltaic properties of PSCs based on bridging polymers from the previous literature and our study are listed in Table 3. It is seen that the device based on our synthesized hyperbranched **P2** shows much higher J_{SC} and *PCE* values compared with other works. To the best of our knowledge, the synthesized DPP-containing **P2** in this study demonstrates the best

device result among bridging polymers so far.

Table 2. Parameters of inverted PSCs based on **P1**, **P2** and P3HT blended with $PC_{61}BM$ under AM 1.5G illumination at 100 mA/cm^2.

Polymer	V_{OC} (V)	J_{SC} (mA/cm^2)	*FF* (%)	*PCE* (%)
P1	0.57	16.21	40	3.74
P2	0.58	11.29	37	2.38
P3HT	0.55	12.67	36	2.55

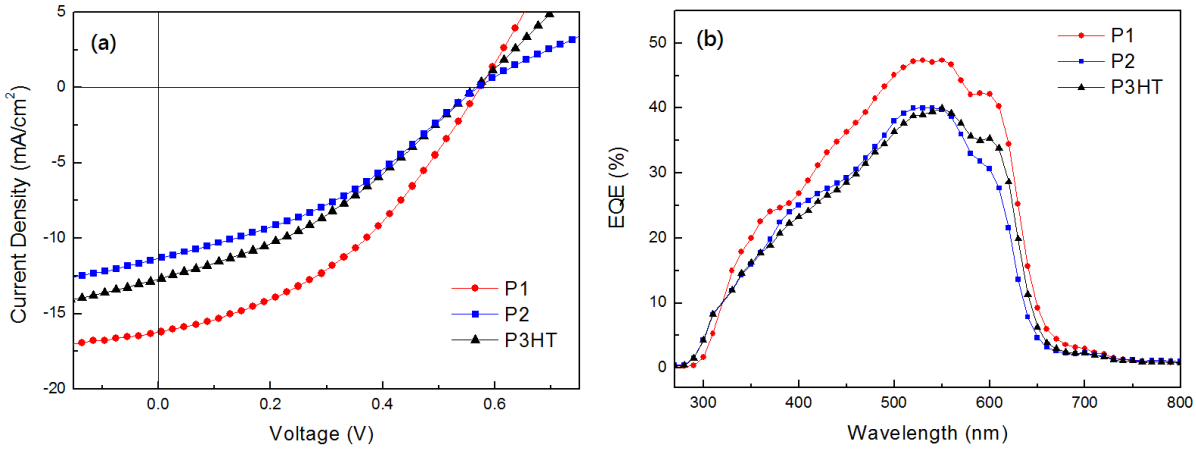

Figure 5. (a) Current density-voltage characteristics and (b) EQE spectra of inverted PSCs based on **P1**, **P2** and P3HT blended with $PC_{61}BM$ under AM 1.5G illumination at 100 mW/cm^2.

Table 3. Comparison of photovoltaic properties of PSCs based on bridging polymers (donor) and $PC_{61}BM$ (acceptor).

Polymer	V_{OC} (V)	J_{SC} (mA/cm^2)	*FF* (%)	*PCE* (%)	Ref
P1	0.57	16.21	40	3.74	this work
P2	0.58	11.29	37	2.38	this work
PT-VTThV	0.67	6.82	38	1.72	[10]
B-P3HT	0.55	N/A [a]	47	2.0	[11]
p-3T-TCM	0.714	2.09	40	0.58	[12]
hyperbranched PT containing PBI	0.72	3.17	37	0.84	[13]

[a] the data was not reported in the literature.

From Table 2 and Figure 5, it is concluded that **P1** shows the best device performance among three polymers in this study, mainly due to larger J_{SC}, *FF* and EQE behavior. Although the **P2** device shows lower J_{SC} value compared with P3HT, the higher V_{OC} and *FF* values make it comparable with

P3HT. To further understand the performance trends of different polymers, we applied the AFM technique for morphological investigations. It is believed that proper phase separation between donor polymer and acceptor $PC_{61}BM$ is the key issue to high-efficiency solar devices [46,47,48]. The AFM topographic images of different polymer:$PC_{61}BM$ blend films are shown in Figure 6. The **P1**:$PC_{61}BM$ blend film shows the most homogeneous dispersion of aggregations, which is beneficial for charge dissociation between electron donor and acceptor. The root-mean-square roughness (R_a) of **P1**:$PC_{61}BM$ blend film is measured to be 7.25 nm that is also better than P3HT and **P2** blend films, revealing R_a values of 8.24 and 11.5 nm, respectively. Combining adequate aggregate distribution and R_a value, the **P1**:$PC_{61}BM$ blend film represents the best surface morphology and film-forming property among three polymer blends, and higher device performance based on this **P1**:$PC_{61}BM$ blend is expected.

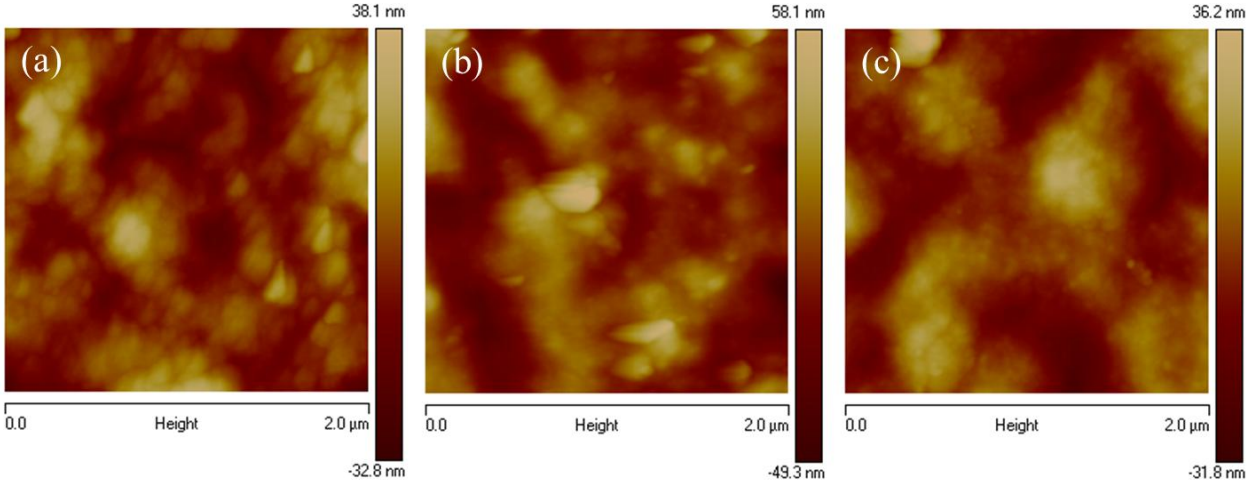

Figure 6. AFM topographic images of (a) **P1**, (b) **P2** and (c) P3HT thin films blended with $PC_{61}BM$.

4. Conclusion

In this research, two different ways for incorporating DPP linking groups to form linear or hyperbranched PT derivatives were proposed and characterized. The effects of introducing DPP groups onto P3HT were investigated by miscellaneous techniques, such as GPC, thermal analysis, optical and electrochemical measurements. The distinct PL decay of DPP-containing polymers in thin film state indicates a more efficient transport process for charge carriers. The lower HOMO levels of polymers resulted from incorporating electron-withdrawing DPP groups brings benefits in increasing V_{OC} values for photovoltaic application. The inverted solar device based on **P1**:$PC_{61}BM$ blend shows high J_{SC} and *PCE* values of 16.21 mA/cm^2 and 3.74%, respectively. The solar device using **P2**:$PC_{61}BM$ blend as the active layer reveals a *PCE* value of 2.38% that demonstrates the highest record among bridging polymers in the literature.

Acknowledgments

The authors gratefully thank to the Ministry of Science and Technology of the Republic of China (NSC 102-2113-M-009-007) for financial support of this work.

Conflict of Interest

All authors declare no conflicts of interest in this paper.

References

1. Loewe RS, Khersonsky SM, McCullough RD (1999) A simple method to prepare head-to-tail coupled, regioregular poly(3-alkylthiophenes) using Grignard metathesis. *Adv Mater* 11: 250–253.
2. Loewe RS, Ewbank PC, Liu J, et al. (2001) Regioregular, head-to-tail coupled poly(3-alkylthiophenes) made easy by the GRIM method: investigation of the reaction and the origin of regioselectivity. *Macromolecules* 34: 4324–4333.
3. Kim Y, Cook S, Tuladhar SM, et al. (2006) A strong regioregularity effect in self-organizing conjugated polymer films and high-efficiency polythiophene:fullerene solar cells. *Nat Mater* 5: 197–203.
4. Cheng YJ, Yang SH, Hsu CS (2009) Synthesis of conjugated polymers for organic solar cell applications. *Chem Rev* 109: 5868–5923.
5. Chang YT, Hsu SL, Chen GY, et al. (2008) Intramolecular donor–acceptor regioregular poly(3-hexylthiophene)s presenting octylphenanthrenyl-imidazole moieties exhibit enhanced charge transfer for heterojunction solar cell applications. *Adv Funct Mater* 18: 2356–2365.
6. Chang YT, Hsu SL, Su MH, et al. (2009) Intramolecular donor–acceptor regioregular poly(hexylphenanthrenyl-imidazole thiophene) exhibits enhanced hole mobility for heterojunction solar cell applications. *Adv Mater* 21: 2093–2097.
7. Hou J, Tan Z, Yan Y, et al. (2006) Synthesis and photovoltaic properties of two-dimensional conjugated polythiophenes with bi(thienylenevinylene) side chains. *J Am Chem Soc* 128: 4911–4916.
8. Li Y, Zou Y (2008) Conjugated polymer photovoltaic materials with broad absorption band and high charge carrier mobility. *Adv Mater* 20: 2952–2958.
9. Zhang Q, Cirpan A, Russell TP, et al. (2009) Donor–acceptor poly(thiophene-*block*-perylene diimide) copolymers: synthesis and solar cell fabrication. *Macromolecules* 42: 1079–1082.
10. Lanzi M, Paganin L, Errani F (2012) Synthesis, characterization and photovoltaic properties of a new thiophene-based double-cable polymer with pendent fullerene group. *Polymer* 53: 2134–2145.
11. Lanzi M, Salatelli E, Benelli T, et al. (2015) A regioregular polythiophene-fullerene for polymeric solar cells. *J Appl Polym Sci* 132: 42121.
12. Piereini F, Lanzi M, Nakielski P, et al. (2017) Single-Material Organic Solar Cells Based on Electrospun Fullerene-Grafted Polythiopene Nanofibers. *Macromolecules* 50: 4972–4981.
13. Zhou E, Tan Z, Yang Y, et al. (2007) Synthesis, hole mobility, and photovoltaic properties of cross-linked polythiophenes with vinylene-terthiophene-vinylene as conjugated bridge. *Macromolecules* 40: 1831–1837.
14. Tu G, Bilge A, Adamczyk S, et al. (2007) The influence of interchain branches on solid state packing, hole mobility and photovoltaic properties of poly(3-hexylthiophene) (P3HT). *Macromol Rapid Comm* 28: 1781–1785.

15. Mangold HS, Richter TV, Link S, et al. (2012) Optoelectronic properties of hyperbranched polythiophenes. *J Phys Chem B* 116: 154–159.
16. Yang SH, Lin TS, Huang YZ, et al. (2014) Synthesis of hyperbranched polythiophenes containing tetrachloroperylene bisimide as bridging moiety for polymer solar cells. *Polymer* 55: 6058–6068.
17. Li W, Hendriks KH, Roelofs WSC, et al. (2013) Efficient small bandgap polymer solar cells with high fill factors for 300 nm thick films. *Adv Mater* 25: 3182–3186.
18. Tan H, Deng X, Yu J, et al. (2013) A novel benzo[1,2-b:4,5-b']dithiophene-based conjugated polymer with a pendant diketopyrrolopyrrole unit for high-performance solar cells. *Macromolecules* 46: 113–118.
19. Kanimozhi C, Balraju P, Sharma GD, et al. (2010) Synthesis of diketopyrrolopyrrole containing copolymers: a study of their optical and photovoltaic properties. *J Phys Chem B* 114: 3095–3103.
20. Huo L, Hou J, Chen HY, et al. (2009) Bandgap and molecular level control of the low-bandgap polymers based on 3,6-dithiophen-2-yl-2,5-dihydropyrrolo[3,4-c]pyrrole-1,4-dione toward highly efficient polymer solar cells. *Macromolecules* 42: 6564–6571.
21. Roncali J (1997) Synthetic principles for bandgap control in linear π-conjugated systems. *Chem Rev* 97: 173–205.
22. Stefan MC, Javier AE, Osaka I, et al. (2009) Grignard metathesis method (GRIM): toward a universal method for the synthesis of conjugated polymers. *Macromolecules* 42: 30–32.
23. Chen WC, Chen PY, Yang SH (2017) Solution-processed hybrid light emitting and photovoltaic devices comprising zinc oxide nanorod arrays and tungsten trioxide layers. *AIMS Mater Sci* 4: 551–560.
24. Huang WJ, Huang PH, Yang SH (2016) PCBM doped with fluorene-based polyelectrolytes as electron transporting layers for improving the performance of planar heterojunction perovskite solar cells. *Chem Commun* 52: 13572–13575.
25. Nunez CM, Chiou BS, Andrady AL, et al. (2000) Solution Rheology of Hyperbranched Polyesters and Their Blends with Linear Polymers. *Macromolecules* 33: 1720–1726.
26. Lee JU, Jung JW, Emrick T, et al. (2010) Synthesis of C_{60}-end capped P3HT and its application for high performance of P3HT/PCBM bulk heterojunction solar cells. *J Mater Chem* 20: 3287–3294.
27. Stevens DM, Qin Y, Hillmyer MA, et al. (2009) Enhancement of the morphology and open circuit voltage in bilayer polymer/fullerene solar cells. *J Phys Chem C* 113: 11408–11415.
28. Zhao Y, Yuan G, Roche P (1995) A calorimetric study of the phase transitions in poly(3-hexylthiophene). *Polymer* 36: 2211–2214.
29. Zhao J, Swinnen A, Assche GV, et al. (2009) Phase diagram of P3HT/PCBM blends and its implication for the stability of morphology. *J Phys Chem B* 113: 1587–1591.
30. Kim Y, Choulis SA, Nelson J, et al. (2005) Device annealing effect in organic solar cells with blends of regioregular poly(3-hexylthiophene) and soluble fullerene. *Appl Phys Lett* 86: 063502.
31. Liao HC, Chantarat N, Chen SY, et al. (2011) Annealing effect on photovoltaic performance of hybrid P3HT/In-Situ grown CdS nanocrystal solar cells. *J Electrochem Soc* 158: E67–E72.
32. Li G, Shrotriya V, Yao Y, et al. (2007) Manipulating regioregular poly(3-hexylthiophene): [6,6]-phenyl-C_{61}-butyric acid methyl ester blends—route towards high efficiency polymer solar cells. *J Mater Chem* 17: 3126–3140.
33. Brown PJ, Thomas DS, Köhler A, et al. (2003) Effect of interchain interactions on the absorption and emission of poly(3-hexylthiophene). *Phys Rev B* 67: 064203.

34. Noriega R, Rivnay J, Vandewal K, et al. (2013) A general relationship between disorder, aggregation and charge transport in conjugated polymers. *Nat Mater* 12: 1038–1044.
35. Yao K, Chen L, Li F, et al. (2012) Cooperative assembly donor–acceptor system induced by intermolecular hydrogen bonds leading to oriented nanomorphology for optimized photovoltaic performance. *J Phys Chem C* 116: 714–721.
36. Kim JY, Lee K, Coates NE, et al. (2007) Efficient tandem polymer solar cells fabricated by all-solution processing. *Science* 317: 222–225.
37. Scharber MC, Mühlbacher D, Koppe M, et al. (2006) Design rules for donors in bulk-heterojunction solar cells—towards 10% energy-conversion efficiency. *Adv Mater* 18: 789–794.
38. Zhu R, Jiang CY, Liu B, et al. (2009) Highly efficient nanoporous TiO_2-polythiophene hybrid solar cells based on interfacial modification using a metal-free organic dye. *Adv Mater* 21: 994–1000.
39. Hou J, Chen TL, Zhang S, et al. (2009) An easy and effective method to modulate molecular energy level of poly(3-alkylthiophene) for high-V_{OC} polymer solar cells. *Macromolecules* 42: 9217–9219.
40. Sekiguchi H, Sekiguchi T (2014) Molecular ordering effect of regioregular poly(3-hexylthiophene) using sulfur K-edge X-ray absorption spectroscopy. *Jpn J Appl Phys* 53: 02BB07.
41. Chen HY, Hou J, Zhang S, et al. (2009) Polymer solar cells with enhanced open-circuit voltage and efficiency. *Nat Photonics* 3: 649–653.
42. Huang JS, Chou CY, Lin CF (2014) Enhancing performance of organic-inorganic hybrid solar cells using a fullerene interlayer from all-solution processing. *Sol Energ Mat Sol C* 6: 466–471.
43. Tan Z, Li L, Cui C, et al. (2012) Solution-processed tungsten oxide as an effective anode buffer layer for high-performance polymer solar cells. *J Phys Chem C* 116: 18626–18632.
44. Lampande R, Kim GW, Boizot J, et al. (2013) A highly efficient transition metal oxide layer for hole extraction and transport in inverted polymer bulk heterojunction solar cells. *J Mater Chem A* 1: 6895–6900.
45. Wang F, Tan Z, Li Y (2015) Solution-processable metal oxides/chelates as electrode buffer layers for efficient and stable polymer solar cells. *Energ Environ Sci* 8: 1059–1091.
46. Ma W, Yang C, Gong X, et al. (2005) Thermally stable, efficient polymer solar cells with nanocontrol of the interpenetrating network morphology. *Adv Funct Mater* 15: 1617–1622.
47. Li G, Shrotriya V, Yao Y, et al. (2005) Investigation of annealing effects and film thickness dependence of polymer solar cells based on poly(3-hexylthiophene). *J Appl Phys* 98: 043704.
48. Peet J, Kim Y, Coates NE, et al. (2007) Efficiency enhancement in low-bandgap polymer solar cells by processing with alkane dithiols. *Nat Mater* 6: 497–500.

AIMS Press